HHS Public Access

Author manuscript

Hum Mutat. Author manuscript; available in PMC 2015 October 01.

Published in final edited form as:

Hum Mutat. 2014 October ; 35(10): 1153–1162. doi:10.1002/humu.22618.

Mutation of *POC1B* in a severe syndromic retinal ciliopathy

Bodo B. Beck[1], **Jennifer B. Phillips**[2], **Malte P. Bartram**[3], **Jeremy Wegner**[2], **Michaela Thoenes**[1], **Andrea Pannes**[1], **Josephina Sampson**[4], **Raoul Heller**[1], **Heike Göbel**[5], **Friederike Koerber**[6], **Antje Neugebauer**[7], **Andrea Hedergott**[7], **Gudrun Nürnberg**[8], **Peter Nürnberg**[8,9], **Holger Thiele**[8], **Janine Altmüller**[1,8], **Mohammad R. Toliat**[8], **Simon Staubach**[1], **Kym M. Boycott**[10], **Enza Maria Valente**[11,12], **Andreas R. Janecke**[13], **Tobias Eisenberger**[14], **Carsten Bergmann**[14,15], **Lars Tebbe**[16], **Yang Wang**[17], **Yundong Wu**[17,18], **Andrew M. Fry**[4], **Monte Westerfield**[2], **Uwe Wolfrum**[16,19], and **Hanno J. Bolz**[1,14]

[1]Institute of Human Genetics, University Hospital of Cologne, 50931 Cologne, Germany

[2]Institute of Neuroscience, University of Oregon, 97401 Eugene, Oregon, USA

[3]Department II of Internal Medicine and Center for Molecular Medicine Cologne, University Hospital of Cologne, 50931 Cologne, Germany

[4]Department of Biochemistry, University of Leicester, Leicester, United Kingdom, LE7 9HN

[5]Department of Pathology, University Hospital of Cologne, 50931 Cologne, Germany

[6]Department of Radiology, University Hospital of Cologne, 50931 Cologne, Germany

[7]Department of Ophthalmology, University Hospital of Cologne, 50931 Cologne, Germany

[8]Cologne Center for Genomics (CCG) and Centre for Molecular Medicine Cologne (CMMC), University of Cologne, 50931 Cologne, Germany

[9]Cologne Excellence Cluster on Cellular Stress Responses in Aging-Associated Diseases (CECAD), University of Cologne, 50931 Cologne, Germany

[10]Children's Hospital of Eastern Ontario Research Institute, University of Ottawa, K1H 8L1 Ottawa, Canada

Correspondence to: Hanno J. Bolz; Fax: 00496132-781298; Phone: 004915228107171; hanno.bolz@uk-koeln.de.

CONFLICT OF INTEREST STATEMENT

T.E., C.B. and H.J.B. are employees of Bioscientia which is part of a publicly traded diagnostic company. The other authors have no competing interests.

NOTE ADDED IN PROOF

Another group simultaneously identified p.Arg106Pro*POC1B* in patients with arCORD, homozygous and *in trans* with an in-frame 1-residue deletion, respectively [Roosing et al., 2014], reinforcing an essential role of POC1B in retinal photoreceptor integrity and function. Of note, they demonstrated interaction of POC1B with FAM161A, confirming our assumption deduced from photoreceptor connecting cilium shortening in both the Poc1b zebrafish model in our study and the recently described *Fam161* mouse model [Karlstetter et al., 2014].

Karlstetter M, Sorusch N, Caramoy A, Dannhausen K, Aslanidis A, Fauser S, Boesl MR, Nagel-Wolfrum K, Tamm ER, Jagle H, Stoehr H, Wolfrum U et al. 2014. Disruption of the retinitis pigmentosa 28 gene Fam161a in mice affects photoreceptor ciliary structure and leads to progressive retinal degeneration. Hum Mol Genet.

Roosing S, Lamers IJC, de Vrieze E, van den Born LI, Lambertus S, Arts HH, Group PBS, Peters TA, Hoyng CB, Kremer H, Hetterschijt L, Letteboer SJF et al. 2014. Disruption of the basal body protein POC1B results in autosomal-recessive cone-rod dystrophy. Am J Hum Genet in press.

[11]Mendel Laboratory, IRCCS Casa Sollievo della Sofferenza Institute, 71013 San Giovanni Rotondo, Italy

[12]Department of Medicine and Surgery, University of Salerno, 84080 Salerno, Italy

[13]Department of Pediatrics I, and Division of Human Genetics, Innsbruck Medical University, 6020 Innsbruck, Austria

[14]Center for Human Genetics, Bioscientia, 55218 Ingelheim, Germany

[15]Department of Medicine, Renal Division, University of Freiburg Medical Center, 79095 Freiburg, Germany

[16]Department of Cell and Matrix Biology, Institute of Zoology, Johannes Gutenberg, University of Mainz, 55099 Mainz, Germany

[17]Lab of Computational Chemistry and Drug Design, Laboratory of Chemical Genomics, Peking University Shenzhen Graduate School, 518000 Shenzhen, P. R. China

[18]College of Chemistry, Peking University, 100871 Beijing, P. R. China

[19]Focus Program Translational Neurosciences (FTN), Johannes Gutenberg University of Mainz, 55122 Mainz, Germany

Abstract

We describe a consanguineous Iraqi family with Leber congenital amaurosis (LCA), Joubert syndrome (JBTS), and polycystic kidney disease. Targeted NGS for excluding mutations in known LCA and JBTS genes, homozygosity mapping and whole-exome sequencing identified a homozygous missense variant, c.317G>C (p.Arg106Pro), in *POC1B*, a gene essential for ciliogenesis, basal body and centrosome integrity. *In silico* modeling suggested a requirement of p.Arg106 for formation of the third WD40 repeat and a protein interaction interface. In human and mouse retina, POC1B localized to the basal body and centriole adjacent to the connecting cilium of photoreceptors and in synapses of the outer plexiform layer. Knockdown of *Poc1b* in zebrafish caused cystic kidneys and retinal degeneration with shortened and reduced photoreceptor connecting cilia, compatible with the human syndromic ciliopathy. A recent study describes homozygosity for p.Arg106Pro$_{POC1B}$ in a family with non-syndromic cone-rod dystrophy. The phenotype associated with homozygous p.Arg106Pro$_{POC1B}$ may thus be highly variable, analogous to homozygous p.Leu710Ser in *WDR19* causing either isolated retinitis pigmentosa or Jeune syndrome. Our study indicates that *POC1B* is required for retinal integrity, and we propose *POC1B* mutations as a probable cause for JBTS with severe polycystic kidney disease.

Keywords

POC1B; LCA; Joubert syndrome; ciliopathy; zebrafish

INTRODUCTION

Leber congenital amaurosis (LCA; MIM# 204000) is characterized by blindness or severe visual impairment at birth or within the first months of life. Infantile severe cone-rod- or

cone dystrophy (CORD, COD) and retinitis pigmentosa (RP) may be clinically indistinguishable from LCA. About 30 LCA genes are known whose (mostly recessive) mutations lead to photoreceptor cell death and account for, depending on the population, at least 62% of cases [Eisenberger et al., 2013]. Many LCA genes encode proteins of the photoreceptor's connecting cilium, a structure that, together with the outer segment, corresponds to a highly specialized primary cilium [Wheway et al., 2013]. Several syndromic ciliopathies, including Joubert syndrome (JBTS; MIM# 213300), are allelic to LCA. JBTS is a rare, mostly autosomal recessive developmental disorder with a characteristic midbrain-hindbrain malformation ("molar tooth sign"), ataxia, psychomotor delay, oculomotor apraxia, and an altered respiratory pattern in the neonatal period. Several other organs apart from the brain may be affected: Most common are retinal degeneration either as LCA or RP; renal cysts, typically as nephronophthisis (NPHP); liver fibrosis; and skeletal involvement, e.g. polydactyly. All known JBTS genes play a role in the formation or function of primary cilia and/or associated structures like the basal body and the centrosomes [Romani et al., 2013]. Here, we report the identification of a mutation in *POC1B* (MIM# 614784) that encodes a core centriole component essential for basal body stability and ciliogenesis in a family with LCA, JBTS and atypical polycystic kidney disease (PKD). Our findings indicate a crucial role of POC1B for retinal function, supported by a recent independent study on a family with autosomal recessive non-syndromic CRD caused by the same *POC1B* mutation [Durlu et al., 2014].

MATERIALS AND METHODS

Ethical approval

Blood samples for DNA extraction were obtained with written informed consent. All investigations were conducted according to the Declaration of Helsinki, and the study was approved by the institutional review board of the Ethics Committee of the University Hospital of Cologne.

Exclusion of mutations in known disease genes

NGS for a gene panel covering 21 JBTS genes, 76 genes associated with autosomal recessive and/or dominant RP, and 27 LCA genes, was carried out on an Illumina HiSeq1500 platform. Enrichment and filtering of data were carried out as described previously, and we applied quantitative readout of NGS reads [Eisenberger et al., 2013]. We thereby excluded large structural rearrangements such as exon deletions or duplications, with special attention to *NPHP1* (homozygous deletion of *NPHP1* is a common cause of JBTS with NPHP [Hildebrandt et al., 1997]) and *CEP290* (which is contained in one of the mapped candidate regions). *PKHD1* was analyzed by direct sequencing of all coding exons.

Homozygosity mapping and whole-exome sequencing (WES)

Genome-wide linkage analysis was carried out with DNA from the index patient, his brother and his parents, using the Illumina HumanCoreExome-12v1-1 BeadChip (Illumina Inc., San Diego, CA) according to the manufacturer's protocol. Linkage analysis was performed assuming autosomal recessive inheritance, full penetrance, consanguinity and a disease gene frequency of 0.0001. Multipoint LOD scores were calculated using the program ALLEGRO

[Gudbjartsson et al., 2000]. All data handling was done using the graphical user interface ALOHOMORA [Rüschendorf and Nürnberg, 2005]. WES and mapping of reads was carried out as previously described [Basmanav et al., 2014]. Filtering and variant prioritization was performed using the Cologne Center for Genomics' VARBANK database and analysis tool (https://varbank.ccg.uni-koeln.de). In particular, we filtered for high-quality (coverage >15-fold; phred-scaled quality >25), rare (MAF (minor allele frequency)≤0.001), homozygous variants (dbSNP build 135, the 1000 Genomes database build 20110521, and the public Exome Variant Server, NHLBI Exome Sequencing Project, Seattle, build ESP6500). To exclude pipeline-related artefacts (MAF≤0.01), we filtered against variants from in-house WES datasets from 511 epilepsy patients. Because our index patient comes from a consanguine background, we also filtered for variants contained in runs of homozygosity. Although compound heterozygous mutations are less likely to be the cause of disease in this family, we also filtered for genes carrying at least two rare variants in the index patient (Supp. Table S1).

Mutation analysis

Confirmation of the homozygous c.317G>C (p.Arg106Pro) mutation in *POC1B* and segregation analysis were carried out by Sanger sequencing. For mutation screening, we searched WES datasets from 19 unrelated JBTS patients without mutations in known disease genes for *POC1B* variants. In four JBTS patients with ocular-renal disease expression, we PCR-amplified the 12 protein-coding exons (GenBank accession number NM_172240.2), followed by Sanger sequencing. Primers and PCR conditions are available on request. The *POC1B* mutation described in this manuscript has been submitted to the Leiden Open Variation Database (LOVD v.3.0), http://www.lovd.nl/POC1B.

In silico assessment of the p.Arg106Pro mutation and the p.Arg106Gln polymorphism (rs76216585)

Evolutionary conservation of the p.Arg106 residue was determined by alignment of the respective peptide stretches from seven species using ClustalW2 (https://www.ebi.ac.uk/Tools/msa/clustalw2). The structure of POC1B was predicted using an algorithm we recently developed, the WD40 structure predictor, WDSP [Wang et al., 2013]. Modeling of POC1B structure was also carried out for a rare dbSNP-annotated variant that affects the same nucleotide position as c.317G>C (rs76216585; c.317G>A), which leads to a different missense variant, p.Arg106Gln.

Endogenous expression of mutant POC1B and immunofluorescence staining of *POC1B* in transfected HEK293T cells

Lymphoblastoid cell lines (LCL) from patient V:12 and his father were generated following standard protocols. POC1B expression was assessed in lysates from LCL, HepG2 cells, and POC1B–transfected HEK293T cells. Cells were harvested in Laemmli buffer, and protein from whole cell lysates was separated on 10% acrylamide gels in tris-glycine buffer (SDS-PAGE). Anti-POC1A/B [Hames et al., 2008] diluted 1:500 to probe membranes for 2 hrs, and HRP-conjugated anti-rabbit IgG secondary antibodies (Dako, Agilent Technologies, Santa Clara, CA), diluted 1:4,000, were used to analyse POC1 expression. The human

h*POC1B*–WT.eGFP plasmid was generated by PCR amplification and subcloning of hPOC1B with an EST-clone as template (BC026080; MRC geneservice, Cambridge, UK) into pEGFP-N1 (Clontech, Takara, Kyoto, Japan) as described before [Hames et al., 2008]. The mutation p.Arg106Pro was introduced using Quickchange mutagenesis according to standard protocols and confirmed by sequencing of the mutant plasmid, h*POC1B*–R106P.eGFP. Cells from the human embryonic kidney cell line 293T (HEK 293T) were maintained in DMEM (Dulbecco's modified Eagle's medium) supplemented with 10% FBS (fetal bovine serum), seeded onto coverslips and then transfected with the indicated plasmids using Lipofectamine2000 (Invitrogen, Life Technologies, Carlsbad, CA). 24 hours after transfection cells were rinsed with PBS several times and fixed with 4% PFA for 10 min. After blocking with 5% normal donkey serum and 0.1% Triton X-100 in dPBS, cells were sequentially stained with rabbit anti-pericentrin (pAB, Abcam (Cambridge, UK), ab4448; primary antibody) and Cy3-conjugated anti-rabbit-IgG (Jackson ImmunoResearch (West Grove, PA): secondary antibody). Coverslips were mounted with Prolong Gold (Invitrogen) and subjected to immunofluorescence microscopy. Pictures were taken with an Axiovert 200 microscope (objective: C-Apochromat 63×/1.22 W) equipped with an Axiocam MRm and the Apotome system (Carl Zeiss MicroImaging, Jena, Germany) using Axiovision 4.8 for acquisition and subsequent image processing (Carl Zeiss MicroImaging).

Determination of POC1B localization in the human retina

Eyes from a healthy human donor (#199-10; aged 56, dissection 29 hours *post mortem*) were obtained from the Department of Ophthalmology, Mainz, Germany, and guidelines to the declaration of Helsinki were followed. All animal experiments conform to the statement by the Association for Research in Vision and Ophthalmology (ARVO) as to care and use of animals in research. Adult C57BL/6J mice were maintained under a 12 hour light–dark cycle, with food and water ad libitum. After sacrifice eyeballs were dissected, cryofixed, sectioned, and immunolabeled as previously described [Overlack et al., 2011]. For indirect immunohistochemical experiments primary antibodies monoclonal antibodies to centrin-3 were used as a molecular marker for the ciliary apparatus of photoreceptors [Trojan et al., 2008], and polyclonal antibodies to POC1B were purchased from Atlas (Stockholm, Sweden). Washed cryosections were incubated with antibodies conjugated to Alexa 488 or Alexa 568 (Invitrogen) in PBS with DAPI (Sigma-Aldrich, St. Louis, MO) to stain the DNA in nuclei and mounted in Mowiol 4.88 (Hoechst, Frankfurt, Germany). Specimens were analyzed in a Leica LEITZ DM6000B deconvolution microscope (Leica, Wetzlar, Germany). Image contrast was adjusted with Adobe Photoshop CS using different tools including color correction.

Zebrafish experiments

All experiments were approved and performed in accordance with guidelines specified by the University of Oregon IACUC. Morpholino oligonucleotides (GeneTools (Philomath, OR), sequences published in [Pearson et al., 2009]) were injected into one-cell stage embryos obtained from Oregon AB X TU mating crosses. Total RNA was extracted from pooled samples of five morpholino-injected or control embryos using the Qiagen RNeasy Kit. Reverse transcription reactions were performed using the SuperScript III Reverse Transcriptase kit (Invitrogen). Transcript variants were detected by PCR using cDNA from

the reverse transcription and previously described primers [Pearson et al., 2009]. PCR fragments were sequenced (Genewiz, South Plainfield, NJ) and analyzed using Lasergene software. Cryosectioning and histology was performed as described [Phillips et al., 2013] with the following primary antibody dilutions: anti-acetylated tubulin (Santa Cruz Biotechnology, Santa Cruz, CA) 1:1000; Anti-active caspase 3 (BD Pharmingen, San Diego, CA) 1:500; Anti-actin (MAB1501, Sigma); Zpr-1 (Zebrafish International Resource Center, Eugene, OR): 1:500. Alexa-fluor 568 Goat anti-rabbit and 488 goat anti-mouse secondary antibodies (Life Technologies) were used at dilutions of 1:1000. Whole larvae images were obtained on a Leica dissecting microscope mounted with a Zeiss Axiocam. Fluorescent and DIC images from sectioned tissue were obtained using a Zeiss LSM5 Confocal microscope. Single plane or compressed z-stacks were analyzed for quantitative data on cilia and cell morphology. 8–10 eyes were analyzed for each category and statistical significance was calculated using an unpaired t-test.

Renal histology

Kidney tissue was available from right sided nephrectomy at the time of living related kidney transplantation. Kidney tissue blocks were fixed in formaldehyde, dehydrated, embedded in paraffin, sectioned at 1–2 μm and assessed by routine staining (Hematoxylin-eosin (H&E), Periodic acid-Schiff (PAS)).

RESULTS

Patient phenotypes

The index patient (V:12), is a 9½-year-old boy, the second child of consanguineous Iraqi parents (Fig. 1A, Fig. 2A). Oligohydramnios and enlarged kidneys were noted at gestational week 22. Patient V:12 was born at 35 weeks by Caesarean section with massively enlarged polycystic kidneys (Fig. 1C – G), birth weight of 2610 g (P50), length of 44 cm (P3) and head circumference of 34.5 cm (P50). There was no gross facial dysmorphism, polydactyly or heterotaxia. He required intensive care and ventilation immediately after birth. Renal function was severely compromised but improved with conservative management. The patient received a preemptive living related kidney graft from his father at 4.5 years of age to avoid dialysis and associated comorbidities. Liver fibrosis, pancreatic and liver cysts, frequent symptoms of ARPKD, were excluded by tissue biopsy and repeated abdominal imaging. Lack of fixation, horizontal and vertical head nodding were evident at four months of age. Ophthalmological examination revealed no better visual function than fixation to light, slow pupil reaction to light, pendular nystagmus with jerk and rotatory components, and no response in visually evoked potentials and electroretinography, compatible with LCA. Eye movements indicated oculomotor apraxia, and a seesaw nystagmus, both typical of JBTS. Fundus examination revealed a small coloboma next to the papilla (right) and small vessel diameter (both eyes). Cranial MRI revealed an MTS (cerebellar vermis hypoplasia, thick and maloriented superior cerebellar peduncles, abnormally deep interpeduncular fossa; Fig. 1B). The patient is mentally retarded. There were at least four additional similarly affected individuals in the family (Fig. 2A) with massively enlarged polycystic kidneys who all died from lung hypoplasia and/or endstage renal disease (ESRD) between neonatal and early school age. Blindness, ataxia, and mental retardation were

reported in two girls (IV:1, IV:6) who died at the ages of 6½ and 9 years, respectively. Two affected boys (V:1, V:2) died too early (one and two days after birth) for blindness to be recognized clinically (clinical synopsis in Supp. Table S2).

Genetic investigations

Next-generation sequencing (NGS) of 21 JBTS genes (except *CSPP1*, which has only recently been reported), 76 RP and 27 LCA genes, did not identify any point mutations or large structural rearrangements (quantitative analysis of NGS reads, [Eisenberger et al., 2013]). Testing for homozygous deletion of *NPHP1*, a common cause of JBTS with NPHP, and direct sequencing of *PKHD1*, the only known ARPKD gene, revealed no mutation. Assuming a homozygous recessive mutation, we carried out genome-wide linkage analysis, based on DNA from the index patient, his brother and his parents. We identified twelve regions of homozygosity by descent (HBD) with a combined maximum parametric LOD score of 1.33 on chromosomes 2 (2×), 6, 7, 9, 10, 12, 13, 15, 17 (2×) and 19 (Fig. 2B). Subsequent whole-exome sequencing (WES) for a sample of the index patient (mean coverage of 101-fold (30-fold for 90%, and 10-fold for 97% of target sequences, respectively)) revealed 19 homozygous candidate variants in the HBD regions (Supp. Table S3). We queried the Ciliaproteome database (V3) [Gherman et al., 2006] and Pubmed for the genes with these rare variants: Only two genes, *ABCB6* and *POC1B* (also called *WDR51B* and *PIX1*; MIM# 614784), each carrying a homozygous missense variant, had documented ciliary expression. In contrast to the POC1B variant, the *ABCB6* variant p.Leu425Val (c.1273C>G) has been annotated in dbSNP (rs111852229; MAF: C=0.001/3). No MAF was available for p.Arg106Pro (c.317G>C) in *POC1B* (RefSeq accession number NM_172240.2). Bioinformatic programs predict pathogenicity of this variant in exon 4 of *POC1B* (Fig. 2C), which affects an evolutionarily highly conserved position (Fig. 2D, Supp. Table S2). While *ABCB6* mutations cause the recessive Lan(−) blood group phenotype [Helias et al., 2012] or dominant ocular coloboma [Wang et al., 2012], mutations in a protein closely related to POC1B, POC1A (MIM# 614783), underlie two similar recessive ciliopathies (with a truncation causing primordial dwarfism [Shaheen et al., 2012], and a missense mutation underlying short stature, onychodysplasia, facial dysmorphism and hypotrichosis (SOFT) syndrome [Sarig et al., 2012]). We thus focused on *POC1B* as the likely disease gene. Segregation analysis including recently obtained samples from 10 additional healthy family members was compatible with a causative role of the *POC1B* mutation; all six consanguineous parents of affected individuals (IV:1, IV:6; V:1, V:2, V:12) were heterozygous carriers (Fig. 2A,D). The LOD score for c.317G>C in *POC1B*, considering the extended segregation analysis, was 2.61, compared to 1.33 for the 12 HBD regions from initial linkage analysis (Fig. 2B). 18 genes, including five with documented or likely ciliary expression, were found to carry at least two rare variants (Supp. Table S1). However, none of these genes appeared to be a convincing candidate for disease in our family (mutated in unrelated diseases; pathogenicity unlikely based on bioinformatic predictions; documented MAFs in general population).

Prediction of WD40 structure in wild-type, mutant and variant POC1B protein

The p.Arg106Pro mutation affects an evolutionarily highly conserved residue of POC1B (Fig. 2E). We predicted the structure of POC1B using the WD40 structure predictor [Wang

et al., 2013]. The seven WD40 blades are well defined in the wild-type protein (Fig. 3A), each exhibiting a β-bulge formed between the beginning of strand a and the end of strand b ($WD_{b\text{-}a}$ bulge) [Wu et al., 2012]. The side chains of several residues, including p.Arg106, extrude from the top face of the propeller and are putative hotspots for protein-protein interaction [Wang et al., 2013; Wu et al., 2012]. Proline is known to disrupt β-sheets and, not allowing an inter-strand hydrogen bond, is very rare in β-bulge structures. The p.Arg106Pro mutation is thus expected to perturb the structure of the top face of the protein (Fig. 3B), to destabilize the protein and to compromise protein-protein interactions [Wu et al., 2012]. In contrast, the known p.Arg106Gln variant (SNP rs76216585) has only a minor effect on structure because the side chains of Arg and Gln are both extended (Fig. 3C). Furthermore, the assumed salt bridge between p.Arg106 and p.Glu122 in the wild-type protein would likely be replaced by a hydrogen bond between p.Gln106 and p.Glu122 in the variant protein. In the p.Arg106Pro mutant, such an electrostatic stabilization is predicted to be absent, supporting the interpretation that a proline residue (but not glutamine) at position 106 of the POC1B protein is disease-causing.

Endogenous expression and centrosomal localization of mutant POC1B in transfected HEK293T cells correspond to wild-type protein

As determined by Western blot, POC1B expression in lymphoblastoid cell lines from patient V:12 appeared normal compared to wild-type cells (data not shown). In HEK293T cells transfected with a plasmid containing the p.Arg106Pro mutation, the protein localized normally at the centrosome (Supp. Fig. S1).

Localization of POC1B in the human retina

We analyzed the distribution of POC1B in the retina by labeling donor human retina from a 56-year old healthy individual and sections of BI6 mouse retina with POC1B antibodies. In both, POC1B was detected predominantly in the ciliary region of photoreceptor cells and synapses of the outer plexiform layer (Fig. 4A; mouse data not shown). Indirect immunofluorescence double labeling with antibodies against POC1B and centrin-3 (a molecular marker of the connecting cilium, the basal body (mother centriole) and the daughter centriole adjacent to the cilium) and high magnification of merged images revealed POC1B localization in the periciliary region at the basal body and the adjacent centriole of the photoreceptor cilium (Fig. 4B,C; scheme in Fig. 4D).

Knockdown of *Poc1b* in zebrafish

Using previously published morpholino oligonucleotides (both translation and splice blocking) to knock down *poc1b* in zebrafish larvae (Fig. 5, Supp. Fig. S2) confirmed the reported ciliopathy phenotype [Pearson et al., 2009] with overall reduced eye size, heart edema, curved tail, abnormal melanocyte distribution and large pronephric cysts (Fig. 5B) which were also detectable in histological sections (Fig. 5D). Most animals did not survive past 5 days post fertilization (dpf). Sectioned retinas from 4 and 5 dpf larvae showed intact retinal structure with distinct cell and plexiform layers (Fig. 5 E–J), but increased cell death throughout the retina (Fig. 5 F). The outer nuclear layer thickness of 4 dpf *poc1b* morphants was not significantly different from that of controls (10.31±0.122 μm and 10.39±0.134 μm,

respectively; p=0.69). However, both the number and length of connecting cilia in the region of the central retina immediately dorsal to the optic nerve were reduced in morphants (Fig. 5 I). *poc1b* retinas had an average of 50 ± 2.02 connecting cilia in this region compared to 74 ± 3.96 in controls (p<0.0001), and an average cilia length of 1.29 ± 0.08 μm compared to 1.98 ± 0.06 μm in controls (p<0.0001). We also examined morphology of the red-green double cones (Fig. 5 J). Measuring from the pedicle to the apical inner segment (the limits of the antibody localization), we noted a significant reduction in the apicobasal length of these cells in *poc1b* morphants compared to controls (12.2 ± 1.15 μm and 16.16 ± 1.07 μm, respectively; p<0.0001).

Mutation screening of *POC1B* in a cohort of JBTS patients

We analyzed WES datasets from 19 JBTS patients without mutations in known JBTS genes, and we sequenced the 12 coding exons of *POC1B* in four patients with the cerebello-oculo-renal form of JBTS, but no mutations were identified in this cohort.

DISCUSSION

Humans have two related POC1 (*proteome of centriole 1*) proteins, POC1A and POC1B, that are required for centriole integrity, basal body stability and ciliogenesis [Pearson et al., 2009]. Their depletion leads to loss of centrioles (barrel-shaped structures of nine triplets of highly stabilized microtubules) and aberrant cell division [Venoux et al., 2013]. In the early stage of the cell division cycle, cells have two centrioles that together with surrounding pericentriolar material constitute a centrosome, the site from which most cytoplasmic microtubules are nucleated. As cells progress into S-phase before cell division, the centrioles duplicate to generate two centrosomes (each with two centrioles) that form the poles of the mitotic spindle. If cells exit the cell cycle into a post-mitotic quiescent or differentiated state, the two centrioles migrate to the cell surface where the mother centriole differentiates to the basal body, which contributes to formation of the primary cilium.

POC1 proteins have a conserved structure with an N-terminal WD40 repeat domain, highly conserved 40 – 60 amino acid motifs preferentially ending with a tryptophan (W) and an aspartic acid (D), that are separated by a spacer sequence from the C-terminal coiled coil domain. WD40 repeats are among the most abundant and highly conserved protein domains from bacteria to mammals. They form β-propeller structures, a platform for binding other proteins and maintaining the integrity of the respective protein complex [Migliori et al., 2012]. Through key protein-protein interactions via the WD40 domain, POC1 proteins contribute to formation and maintenance of the basal body and, potentially, the transition zone that assembles between the distal end of the basal body and the axonemal microtubules of the cilium. These are the sites where LCA, NPHP and JBTS proteins are typically located and interact to assemble functional complexes [Sang et al., 2011]. Mutations disrupting WD40 structure in AHI1 and WDR34 cause JBTS [Ferland et al., 2004] and Jeune syndrome [Huber et al., 2013; Schmidts et al., 2013], respectively, indicating the importance of WD40 proteins for ciliary integrity.

POC1B localizes in the periciliary compartment at the basal body and the adjacent centriole of primary cilia of photoreceptors (Fig. 4B,C; scheme in Fig. 4D). This subciliary

compartment is characterized by modules that regulate the delivery of ciliary components into the cilium, namely the BBSome [Nachury et al., 2010]. As in other primary cilia, the molecular components of the intraflagellar transport (IFT) machinery are assembled in this periciliary region of the photoreceptor cilium [Sedmak and Wolfrum, 2010]. This strategic site is a localization hotspot of proteins involved in isolated (e.g. TOPORS, RAB28, RP2, LCA5, FAM161A) and syndromic retinal degeneration (including JBTS with retinal degeneration, e.g. caused by *NPHP1*, *RPGRIP1L* and *OFD1* mutations) [Wheway et al., 2013], and diverse mutations in lebercilin (*LCA5*) disrupt its interactions with the IFT machinery [Boldt et al., 2011]. In *RP28* mice, retinal pathology apparently arises from inability of truncated Fam161a to bind lebercilin and cep290. The shorter connecting cilia in *RP28* mice [Karlstetter et al., 2014] resemble the defects in *poc1B*–deficient zebrafish, and the pathomechanisms of *POC1B*- and *FAM161A*–associated LCA may hence be similar. The p.Arg106Pro mutation does apparently not interfere with endogenous POC1B expression or its centrosomal localization (Supp. Fig. S1). Together with our *in silico* prediction suggesting a perturbation of WD40 structure by p.Arg106Pro (Fig. 3), we speculate that rather than being mislocalized itself, $POC1B_{p.Arg106Pro}$ has lost its ability to bind other proteins required for normal retinal, renal and cerebellar development. Identification of the proteins interacting with POC1B will undoubtedly reveal known ciliopathy proteins and novel candidates for disease, and help understanding the pathomechanisms of *POC1B* deficiency.

Mutations in particular JBTS genes predispose to additional cystic kidney disease (*RPGRIP1L*, *NPHP1*, *CEP290*, *CC2D2A*, *TMEM67*, *TMEM216*, *TMEM237*, *ZNF423*), retinal degeneration (*AHI1*, *CEP290*, *CC2D2A*, *INPP5E*, *OFD1*) or both (*CEP290*, *NPHP1*, *AHI1*, *TMEM231*) [Romani et al., 2013]. Cystic kidney disease in JBTS typically manifests as NPHP, with small to normal-sized kidneys and cysts at the corticomedullary junction, tubular atrophy, interstitial fibrosis and tubular basement membrane changes. ESRD in NPHP occurs variably from infancy to the third decade of life. In the index patient's family, the renal disease is distinctly different from typical NPHP and is instead more reminiscent of ARPKD, based on the clinical course (prenatal onset, renal oligohydramnion, rapid progression to ESRD, lung hypoplasia) as well as macroscopic and imaging observations (massively enlarged polycystic kidneys, lung hypoplasia; Fig. 1C). Only three JBTS children, all carrying *TMEM67* mutations, have been reported with features of both ARPKD and NPHP. In contrast to patient V:12 and his family, they presented with congenital hepatic fibrosis, a symptom frequently found in ARPKD and a subset of NPHP patients, and there were no signs of retinal degeneration [Gunay-Aygun et al., 2009]. Histologically, cysts in patient V:12 appear rounded as in autosomal dominant PKD (ADPKD), but in contrast to ADPKD, cysts are mainly located in cortical and subcortical regions (Fig. 1D). Moreover, patient V:12 has larger kidneys with more and larger cysts than typically found in ADPKD, and the degenerative histological changes (collecting ducts and most parts of the loop of Henle are absent from the medullary region; Fig. 1E) overlap only partially with NPHP and PKD features. Congenital hepatic fibrosis was not present in the family described here. In summary, the index patient's family displays an unusual type of PKD that overlaps with (but clearly differs from) NPHP, ARPKD and ADPKD, and elucidation of the pathomechanism in the family described herein may therefore reveal common pathways for these renal

diseases: *POC1B* malfunction could induce degeneration of medullary tubular structures with secondary cystic hypertrophy resulting in rounded cysts. Alternatively, primary ciliary dysfunction could, as in ADPKD, induce proliferation defects with subsequent cyst formation [Harris and Torres, 2009].

Analysis of WES datasets from 23 unrelated JBTS patients without mutations in known JBTS genes and sequencing of *POC1B* in four patients with cystic kidney disease and retinal degeneration failed to identify additional mutations. None of the screened patients had a PKD phenotype comparable to our family; if the rare combination of atypical PKD with LCA was obligatory for *POC1B*–associated JBTS, this would explain the outcome of mutation screening.

Recently, an independent study reported homozygosity for the same *POC1B* mutation as described in our study, p.Arg106Pro, that caused autosomal recessive non-syndromic CORD in four members of a consanguineous Turkish family [Durlu et al., 2014]. In contrast to our family, none of the patients were blind at birth, and their phenotype (decreased visual acuity, severe photophobia and impaired color vision) was categorized as severe and slowly progressive CORD. The difference in disease severity is not surprising because CORD exhibits wide clinical variability, and early-onset severe CORD may be clinically indistinguishable from LCA. Furthermore, mutations in several genes, e.g. *RPGRIP1*, may cause either LCA or CORD [Hamel, 2007; Khan et al., 2013]. The study by Durlu et al. supports our findings that indicate a crucial role of *POC1B* for retinal function and integrity.

In addition, we propose *POC1B* as a candidate for syndromic retinal dystrophy, JBTS with LCA and PKD. Our findings resemble a similar phenomenon for mutations in another ciliary WD40 protein, WDR19, where homozygosity for the missense mutation p.Leu710Ser has been shown to cause either non-syndromic autosomal recessive RP [Coussa et al., 2013] or a potentially lethal syndromic ciliopathy, Jeune syndrome [Bredrup et al., 2011]. Similarly, compound-heterozygosity for the same truncating mutations in ciliary *IQCB1*, may cause LCA either in isolation [Estrada-Cuzcano et al., 2011] or in conjunction with early renal failure due to nephronophthisis (Senior Loken syndrome) [Otto et al., 2005]. A possible explanation is the effect of modifier alleles in additional ciliary genes. For example, specific alleles of *RPGRIP1L* and *AHI1* have been shown to influence the penetrance of retinal degeneration in ciliopathies [Khanna et al., 2009; Louie et al., 2010]. The *POC1B* mutation p.Arg106Pro may represent a founder allele, and the CORD family [Durlu et al., 2014] and the family with a syndromic retinal ciliopathy reported in our study may be distantly related. Differences in genetic background (due to distinct geographical origins, Turkey and Iraq) could account for disease expression of p.Arg106Pro as CORD in one family and as severe syndromic ciliopathy (JBTS) in the other.

Finally, we cannot exclude the possibility that disease in patients of the Iraqi family described herein results from homozygosity for mutations in at least two genes, with the *POC1B* mutation accounting for non-syndromic retinal dystrophy and a yet unknown mutation for the extraocular symptoms (JBTS, PKD). Because every individual can be expected to carry heterozygous mutations for several recessive conditions, offspring of consanguineous parents may become homozygous for more than one mutation in unlinked

genes, and co-occurence of two recessive conditions may mimick a single, syndromic disorder. We have previously described this in families with suspected Navajo neurohepatopathy and Usher syndrome [Ebermann et al., 2008; Ebermann et al., 2007]. In the WES data of the index patient, there was no indication for such a scenario.

The segregation pattern of the p.Arg106Pro mutation in a large consanguineous family, the consistent phenotype of affected family members, retinal localization of POC1B at sites typical of JBTS/LCA/NPHP proteins and the early lethal renal-retinal ciliopathy phenotype in *poc1b*–deficient zebrafish support the hypothesis that *POC1B* not only causes the retinal degeneration in the family reported here, but also JBTS with PKD. However, further unrelated cases are needed to provide definitive proof for this interpretation.

Supplementary Material

Refer to Web version on PubMed Central for supplementary material.

ACKNOWLEDGMENTS

We are grateful to the families and patients who participated in our study. We thank Gabi Stern-Schneider, Fritz Textoris and Katharina Zimmermann for excellent technical assistance. This work was supported by funding from the Marie-Louise Geissler-Stiftung and the Imhoff-Stiftung to H.J.B.; the Imhoff-Stiftung to B.B.B.; Koeln Fortune, Faculty of Medicine, University of Cologne (172/2013) to S.S.; the NIH (DC004186, DC010447, OD011195 and HD22486) to M.W.; the Deutsche Forschungsgemeinschaft (GRK 1044), the FAUN-Stiftung (Nürnberg), the European Community FP7/2009/241955 (*SYSCILIA*), the BMBF (0314106, *HOPE2*) to U.W.; the NSFC (21133002) to Y.D.W.; Kidney Research UK (RP2/2013) and the Biotechnology and Biological Sciences Research Council (BBSRC; BB/F010702/1) to A.M.F.

REFERENCES

Basmanav FB, Oprisoreanu AM, Pasternack SM, Thiele H, Fritz G, Wenzel J, Grosser L, Wehner M, Wolf S, Fagerberg C, Bygum A, Altmuller J, et al. Mutations in POGLUT1, encoding protein O-glucosyltransferase 1, cause autosomal-dominant Dowling-Degos disease. Am J Hum Genet. 2014; 94:135–143. [PubMed: 24387993]

Boldt K, Mans DA, Won J, van Reeuwijk J, Vogt A, Kinkl N, Letteboer SJ, Hicks WL, Hurd RE, Naggert JK, Texier Y, den Hollander AI, et al. Disruption of intraflagellar protein transport in photoreceptor cilia causes Leber congenital amaurosis in humans and mice. J Clin Invest. 2011; 121:2169–2180. [PubMed: 21606596]

Bredrup C, Saunier S, Oud MM, Fiskerstrand T, Hoischen A, Brackman D, Leh SM, Midtbo M, Filhol E, Bole-Feysot C, Nitschke P, Gilissen C, et al. Ciliopathies with skeletal anomalies and renal insufficiency due to mutations in the IFT-A gene WDR19. Am J Hum Genet. 2011; 89:634–643. [PubMed: 22019273]

Coussa RG, Otto EA, Gee HY, Arthurs P, Ren H, Lopez I, Keser V, Fu Q, Faingold R, Khan A, Schwartzentruber J, Majewski J, et al. WDR19: an ancient, retrograde, intraflagellar ciliary protein is mutated in autosomal recessive retinitis pigmentosa and in Senior-Loken syndrome. Clin Genet. 2013; 84:150–159. [PubMed: 23683095]

Durlu YK, Koroglu C, Tolun A. Novel Recessive Cone-Rod Dystrophy Caused by POC1B Mutation. JAMA Ophthalmol. 2014

Ebermann I, Elsayed SM, Abdel-Ghaffar TY, Nurnberg G, Nurnberg P, Elsobky E, Bolz HJ. Double homozygosity for mutations of AGL and SCN9A mimicking neurohepatopathy syndrome. Neurology. 2008; 70:2343–2344. [PubMed: 18541889]

Ebermann I, Walger M, Scholl HP, Charbel Issa P, Luke C, Nurnberg G, Lang-Roth R, Becker C, Nurnberg P, Bolz HJ. Truncating mutation of the DFNB59 gene causes cochlear hearing

impairment and central vestibular dysfunction. Hum Mutat. 2007; 28:571–577. [PubMed: 17301963]

Eisenberger T, Neuhaus C, Khan AO, Decker C, Preising MN, Friedburg C, Bieg A, Gliem M, Charbel Issa P, Holz FG, Baig SM, Hellenbroich Y, et al. Increasing the yield in targeted next-generation sequencing by implicating CNV analysis, non-coding exons and the overall variant load: the example of retinal dystrophies. PLoS One. 2013; 8:e78496. [PubMed: 24265693]

Estrada-Cuzcano A, Koenekoop RK, Coppieters F, Kohl S, Lopez I, Collin RW, De Baere EB, Roeleveld D, Marek J, Bernd A, Rohrschneider K, van den Born LI, et al. IQCB1 mutations in patients with leber congenital amaurosis. Invest Ophthalmol Vis Sci. 2011; 52:834–839. [PubMed: 20881296]

Ferland RJ, Eyaid W, Collura RV, Tully LD, Hill RS, Al-Nouri D, Al-Rumayyan A, Topcu M, Gascon G, Bodell A, Shugart YY, Ruvolo M, et al. Abnormal cerebellar development and axonal decussation due to mutations in AHI1 in Joubert syndrome. Nat Genet. 2004; 36:1008–1013. [PubMed: 15322546]

Gherman A, Davis EE, Katsanis N. The ciliary proteome database: an integrated community resource for the genetic and functional dissection of cilia. Nat Genet. 2006; 38:961–962. [PubMed: 16940995]

Gudbjartsson DF, Jonasson K, Frigge ML, Kong A. Allegro, a new computer program for multipoint linkage analysis. Nat Genet. 2000; 25:12–13. [PubMed: 10802644]

Gunay-Aygun M, Parisi MA, Doherty D, Tuchman M, Tsilou E, Kleiner DE, Huizing M, Turkbey B, Choyke P, Guay-Woodford L, Heller T, Szymanska K, et al. MKS3-related ciliopathy with features of autosomal recessive polycystic kidney disease, nephronophthisis, and Joubert Syndrome. J Pediatr. 2009; 155:386–392. e1. [PubMed: 19540516]

Hamel CP. Cone rod dystrophies. Orphanet J Rare Dis. 2007; 2:7. [PubMed: 17270046]

Hames RS, Hames R, Prosser SL, Euteneuer U, Lopes CA, Moore W, Woodland HR, Fry AM. Pix1 and Pix2 are novel WD40 microtubule-associated proteins that colocalize with mitochondria in Xenopus germ plasm and centrosomes in human cells. Exp Cell Res. 2008; 314:574–589. [PubMed: 18068700]

Harris PC, Torres VE. Polycystic kidney disease. Annu Rev Med. 2009; 60:321–337. [PubMed: 18947299]

Helias V, Saison C, Ballif BA, Peyrard T, Takahashi J, Takahashi H, Tanaka M, Deybach JC, Puy H, Le Gall M, Sureau C, Pham BN, et al. ABCB6 is dispensable for erythropoiesis and specifies the new blood group system Langereis. Nat Genet. 2012; 44:170–173. [PubMed: 22246506]

Hildebrandt F, Otto E, Rensing C, Nothwang HG, Vollmer M, Adolphs J, Hanusch H, Brandis M. A novel gene encoding an SH3 domain protein is mutated in nephronophthisis type 1. Nat Genet. 1997; 17:149–153. [PubMed: 9326933]

Huber C, Wu S, Kim AS, Sigaudy S, Sarukhanov A, Serre V, Baujat G, Le Quan Sang KH, Rimoin DL, Cohn DH, Munnich A, Krakow D, et al. WDR34 mutations that cause short-rib polydactyly syndrome type III/severe asphyxiating thoracic dysplasia reveal a role for the NF-kappaB pathway in cilia. Am J Hum Genet. 2013; 93:926–931. [PubMed: 24183449]

Karlstetter M, Sorusch N, Caramoy A, Dannhausen K, Aslanidis A, Fauser S, Boesl MR, Nagel-Wolfrum K, Tamm ER, Jagle H, Stoehr H, Wolfrum U, et al. Disruption of the Retinitis Pigmentosa 28 gene Fam161a in mice affects photoreceptor ciliary structure and leads to progressive retinal degeneration. Hum Mol Genet. 2014

Khan AO, Abu-Safieh L, Eisenberger T, Bolz HJ, Alkuraya FS. The RPGRIP1-related retinal phenotype in children. Br J Ophthalmol. 2013; 97:760–764. [PubMed: 23505306]

Khanna H, Davis EE, Murga-Zamalloa CA, Estrada-Cuzcano A, Lopez I, den Hollander AI, Zonneveld MN, Othman MI, Waseem N, Chakarova CF, Maubaret C, Diaz-Font A, et al. A common allele in RPGRIP1L is a modifier of retinal degeneration in ciliopathies. Nat Genet. 2009; 41:739–745. [PubMed: 19430481]

Louie CM, Caridi G, Lopes VS, Brancati F, Kispert A, Lancaster MA, Schlossman AM, Otto EA, Leitges M, Grone HJ, Lopez I, Gudiseva HV, et al. AHI1 is required for photoreceptor outer segment development and is a modifier for retinal degeneration in nephronophthisis. Nat Genet. 2010; 42:175–180. [PubMed: 20081859]

Migliori V, Mapelli M, Guccione E. On WD40 proteins: propelling our knowledge of transcriptional control? Epigenetics. 2012; 7:815–822. [PubMed: 22810296]

Nachury MV, Seeley ES, Jin H. Trafficking to the ciliary membrane: how to get across the periciliary diffusion barrier? Annu Rev Cell Dev Biol. 2010; 26:59–87. [PubMed: 19575670]

Otto EA, Loeys B, Khanna H, Hellemans J, Sudbrak R, Fan S, Muerb U, O'Toole JF, Helou J, Attanasio M, Utsch B, Sayer JA, et al. Nephrocystin-5, a ciliary IQ domain protein, is mutated in Senior-Loken syndrome and interacts with RPGR and calmodulin. Nat Genet. 2005; 37:282–288. [PubMed: 15723066]

Overlack N, Kilic D, Bauss K, Marker T, Kremer H, van Wijk E, Wolfrum U. Direct interaction of the Usher syndrome 1G protein SANS and myomegalin in the retina. Biochim Biophys Acta. 2011; 1813:1883–1892. [PubMed: 21767579]

Pearson CG, Osborn DP, Giddings TH Jr. Beales PL, Winey M. Basal body stability and ciliogenesis requires the conserved component Poc1. J Cell Biol. 2009; 187:905–920. [PubMed: 20008567]

Phillips JB, Vastinsalo H, Wegner J, Clement A, Sankila EM, Westerfield M. The cone-dominant retina and the inner ear of zebrafish express the ortholog of CLRN1, the causative gene of human Usher syndrome type 3A. Gene Expr Patterns. 2013; 13:473–481. [PubMed: 24045267]

Romani M, Micalizzi A, Valente EM. Joubert syndrome: congenital cerebellar ataxia with the molar tooth. Lancet Neurol. 2013; 12:894–905. [PubMed: 23870701]

Rüschendorf F, Nürnberg P. ALOHOMORA: a tool for linkage analysis using 10K SNP array data. Bioinformatics. 2005; 21:2123–2125. [PubMed: 15647291]

Sang L, Miller JJ, Corbit KC, Giles RH, Brauer MJ, Otto EA, Baye LM, Wen X, Scales SJ, Kwong M, Huntzicker EG, Sfakianos MK, et al. Mapping the NPHP-JBTS-MKS protein network reveals ciliopathy disease genes and pathways. Cell. 2011; 145:513–528. [PubMed: 21565611]

Sarig O, Nahum S, Rapaport D, Ishida-Yamamoto A, Fuchs-Telem D, Qiaoli L, Cohen-Katsenelson K, Spiegel R, Nousbeck J, Israeli S, Borochowitz ZU, Padalon-Brauch G, et al. Short stature, onychodysplasia, facial dysmorphism, and hypotrichosis syndrome is caused by a POC1A mutation. Am J Hum Genet. 2012; 91:337–342. [PubMed: 22840363]

Schmidts M, Vodopiutz J, Christou-Savina S, Cortes CR, McInerney-Leo AM, Emes RD, Arts HH, Tuysuz B, D'Silva J, Leo PJ, Giles TC, Oud MM, et al. Mutations in the gene encoding IFT dynein complex component WDR34 cause Jeune asphyxiating thoracic dystrophy. Am J Hum Genet. 2013; 93:932–944. [PubMed: 24183451]

Sedmak T, Wolfrum U. Intraflagellar transport molecules in ciliary and nonciliary cells of the retina. J Cell Biol. 2010; 189:171–186. [PubMed: 20368623]

Shaheen R, Faqeih E, Shamseldin HE, Noche RR, Sunker A, Alshammari MJ, Al-Sheddi T, Adly N, Al-Dosari MS, Megason SG, Al-Husain M, Al-Mohanna F, et al. POC1A truncation mutation causes a ciliopathy in humans characterized by primordial dwarfism. Am J Hum Genet. 2012; 91:330–336. [PubMed: 22840364]

Trojan P, Krauss N, Choe HW, Giessl A, Pulvermuller A, Wolfrum U. Centrins in retinal photoreceptor cells: regulators in the connecting cilium. Prog Retin Eye Res. 2008; 27:237–259. [PubMed: 18329314]

Venoux M, Tait X, Hames RS, Straatman KR, Woodland HR, Fry AM. Poc1A and Poc1B act together in human cells to ensure centriole integrity. J Cell Sci. 2013; 126:163–175. [PubMed: 23015594]

Wang L, He F, Bu J, Zhen Y, Liu X, Du W, Dong J, Cooney JD, Dubey SK, Shi Y, Gong B, Li J, et al. ABCB6 mutations cause ocular coloboma. Am J Hum Genet. 2012; 90:40–48. [PubMed: 22226084]

Wang Y, Jiang F, Zhuo Z, Wu XH, Wu YD. A method for WD40 repeat detection and secondary structure prediction. PLoS One. 2013; 8:e65705. [PubMed: 23776530]

Wheway G, Parry DA, Johnson CA. The role of primary cilia in the development and disease of the retina. Organogenesis. 2013:10.

Wu XH, Wang Y, Zhuo Z, Jiang F, Wu YD. Identifying the hotspots on the top faces of WD40-repeat proteins from their primary sequences by beta-bulges and DHSW tetrads. PLoS One. 2012; 7:e43005. [PubMed: 22916195]

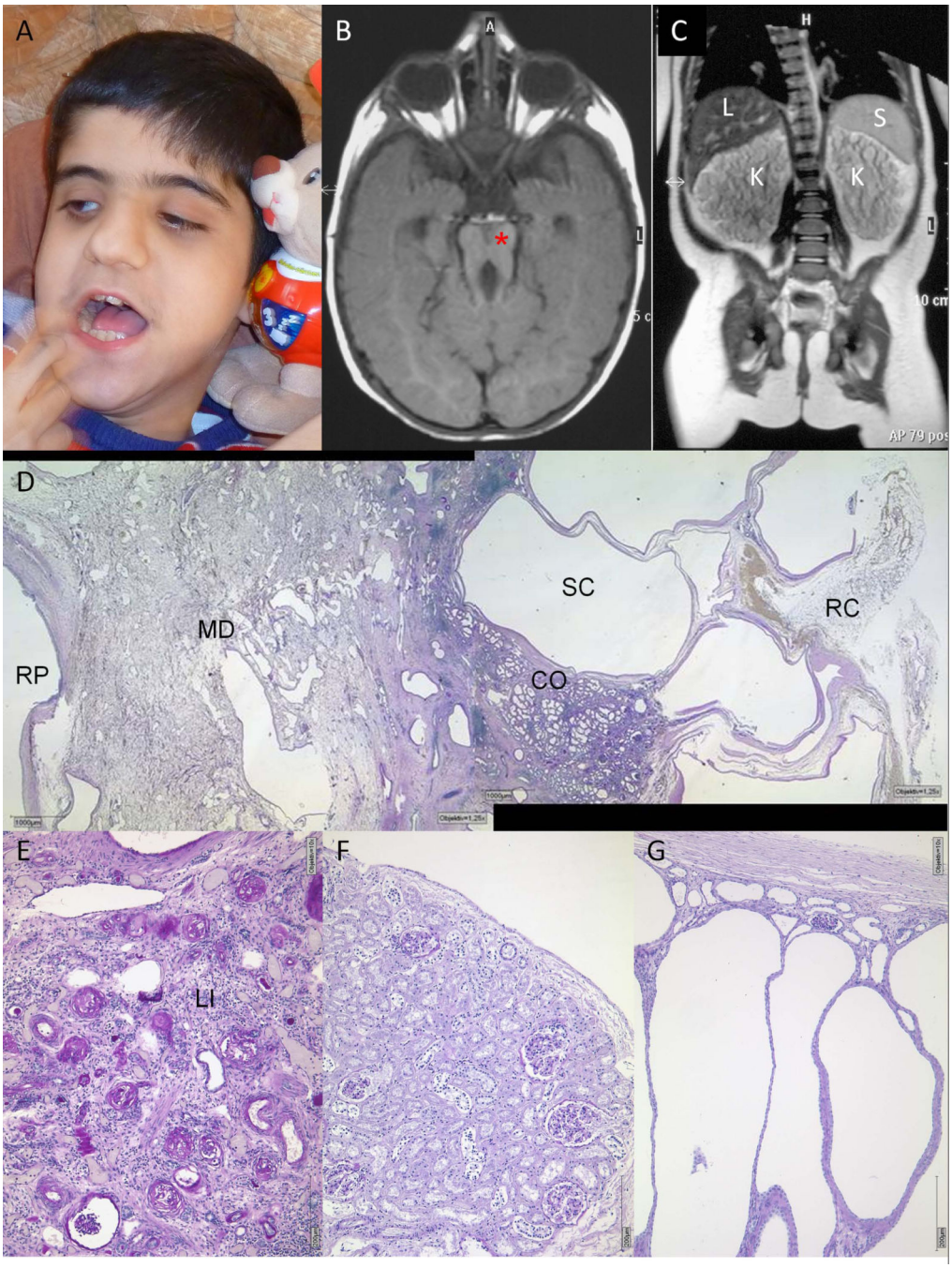

FIGURE 1. Clinical findings in the index patient

A Facial appearance without gross dysmorphology. **B** Axial brain MRI showing molar tooth sign (*). **C** MRI of the trunk showing massively enlarged polycystic kidneys with loss of corticomedullary differentiation. K, kidney; L, liver; S, spleen. **D, E** Specimen from right nephrectomy (269 g; 10,5 × 6,5 × 7,5 cm) at the age of 4.5 years (PAS; D, 12.5×; E, 100×). **D** Overview showing completely abolished tissue architecture with tall (Ø up to 1,2 cm) fluid-filled subcapsular cysts (SC) of tubular origin mainly in cortical (CO) and subcapsular localization. The renal pelvis (RP) was dilated and covered by normal urothelial layer. MD,

medulla; RC, renal capsule. **E** High magnification of cortical region with obsolescent glomeruli, lymphohistioplasmocytic infiltration (LI), severe tubular atrophy and interstitial fibrosis. Hypertrophic tubular structures resemble distal tubuli. Note almost complete absence of collecting ducts and loop of Henle structures in the medullary area (MD). Glomeruli were either normal or compatible with unspecific obsolescence, and arterioles and interlobular arteries appeared normal (not shown). **F** Regular renal cortex (PAS, 100×) for comparison. **G** For comparison, a typical histology of an ARPKD patient (PAS, 100×) is shown with elongated cysts reaching from the cortex to the medulla, separated by loose connective tissue with interspersed glomerular structures.

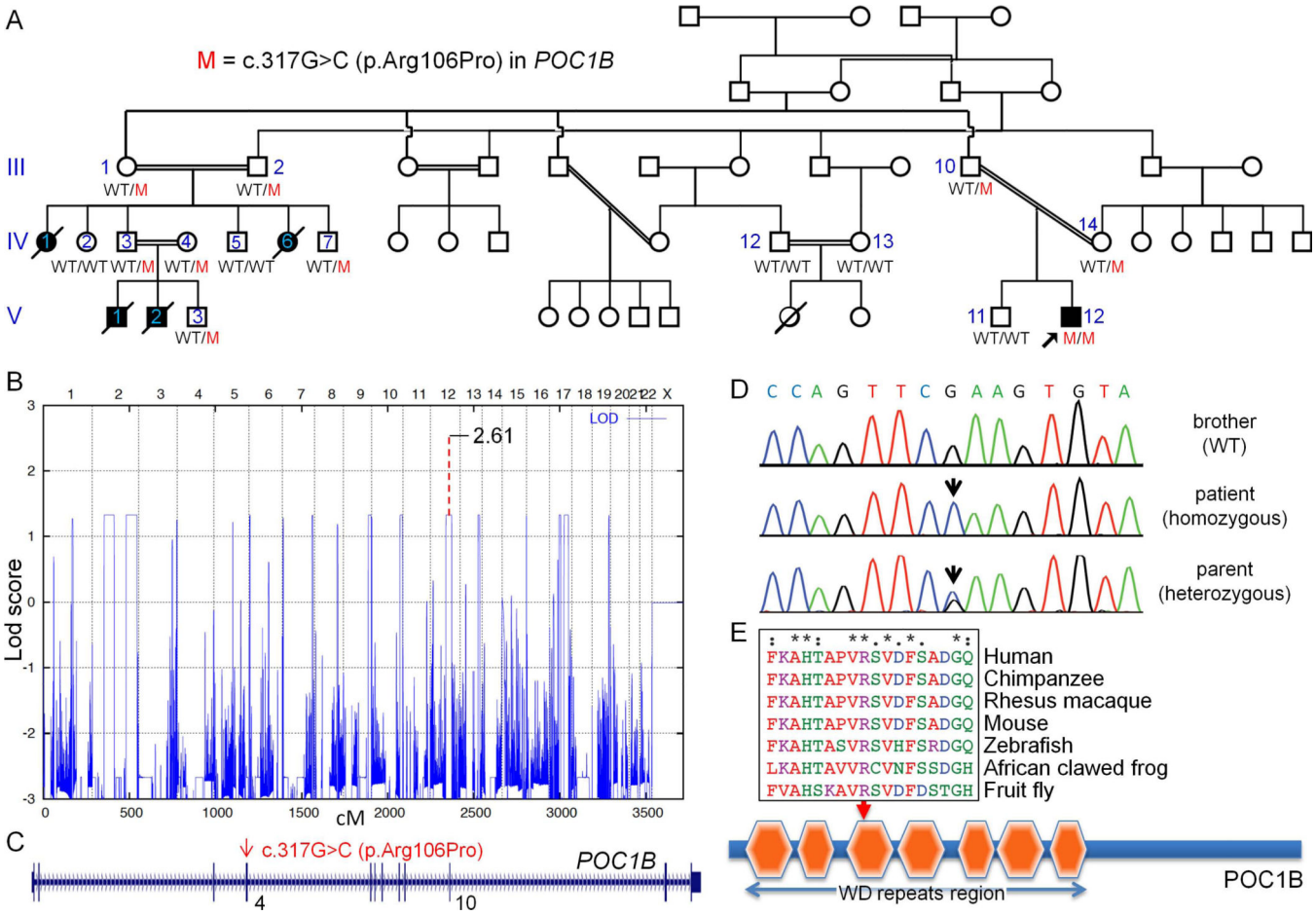

FIGURE 2. Genetic characterization of the consanguineous Iraqi family segregating a *POC1B* mutation

A Pedigree. The sample of the index patient (arrow) was submitted to exome sequencing. For detailed clinical data of the different individuals, see Supp. Table S2. *POC1B* genotypes: WT, wild-type; M, mutant (c.317G>C). **B** Graphical view of the LOD score calculation of genome-wide SNP mapping (based on samples from III:10, IV:14, V:11 and V:12). Regions showing HBD were identified on chromosomes 2 (2×), 6, 7, 9, 10, 12, 13, 15, 17 (2×) and 19. The dotted line indicates the LOD score for c.317G>C in *POC1B* based on genotypes from all finally available samples in the family. **C** Scheme of the *POC1B* gene with the identified mutation. **D** Sanger sequencing confirmed the homozygous mutation, c. 317G>C (p.Arg106Pro) in *POC1B* exon 4, in the patient (middle panel). It was found in heterozygous state in both parents (lower panel), while the healthy brother displayed wild-type sequence (upper panel). Scheme of the POC1B protein with the mutation affecting a evolutionarily highly conserved residue in the third WD40 repeat. For clarity, the one-letter amino acid code was applied for mutation designation in this subset of the figure.

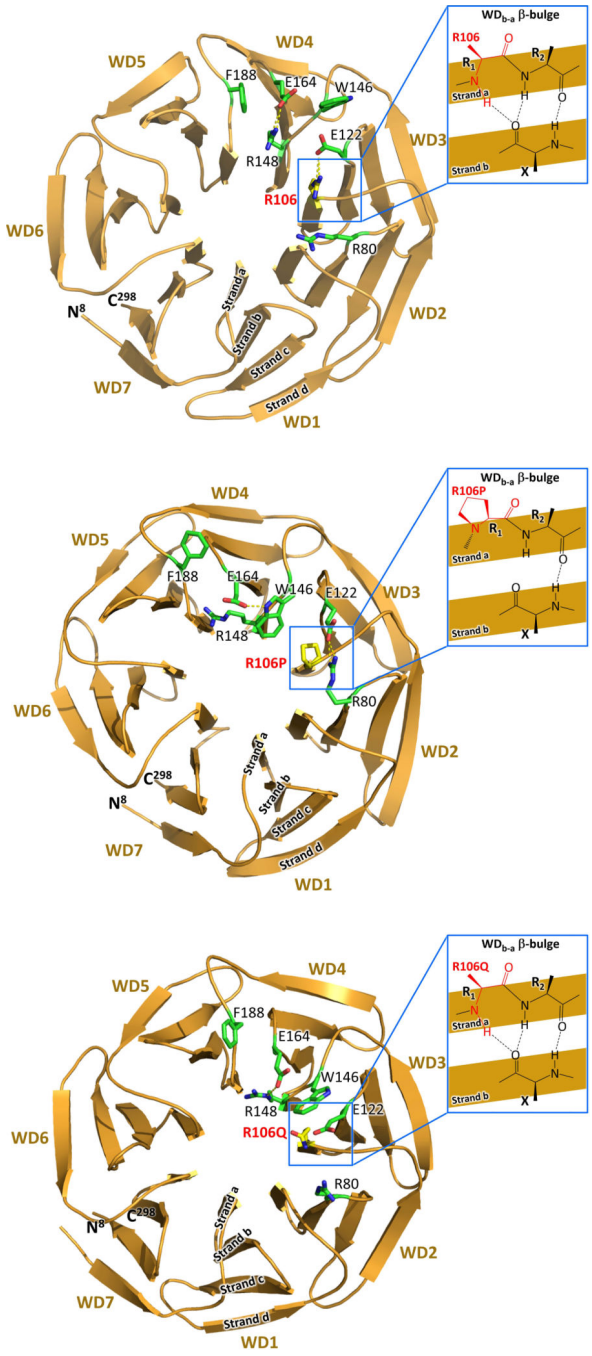

FIGURE 3. Structure of wild-type, mutant and variant POC1B WD40 domain as predicted by the WDSP algorithm

(refined by an 800 ns MD simulation using a residue specific force-field). For simplicity, the one-letter-code is being used for amino acid residues. The strands a–d are depicted in WD1, and the $WD_{b\text{-}a}$ β-bulge is shown for WD3. **A** The seven WD40 blades are well defined in the wild-type, each exhibiting a β-bulge formed between the beginning of strand a and the end of strand b ($WD_{b\text{-}a}$ bulge). The side chain of p.Arg106, which locates at the R_1 position of the bulge in the blade WD3, extrudes on the top face of the propeller. p.Arg106 and several

other residues shown in the figure are predicted to be the potential hotspots for ligand binding. **B** The p.Arg106Pro mutation disrupts the $WD_{b\text{-}a}$ bulge in WD3, perturbs the conformation of p.Trp146, p.Arg80 and p.Glu122 and the ligand binding environment of the top face of the propeller. **C** The known p.Arg106Gln polymorphism (SNP rs76216585) only has a minor effect on structure. The side chains of Arg and Gln are both extended. A hydrogen bond between p.Gln106 and p.Glu122 in the variant protein ould provide electrostatic stabilization, similar the salt bridge between p.Arg106 and p.Glu122 in the wild-type protein.

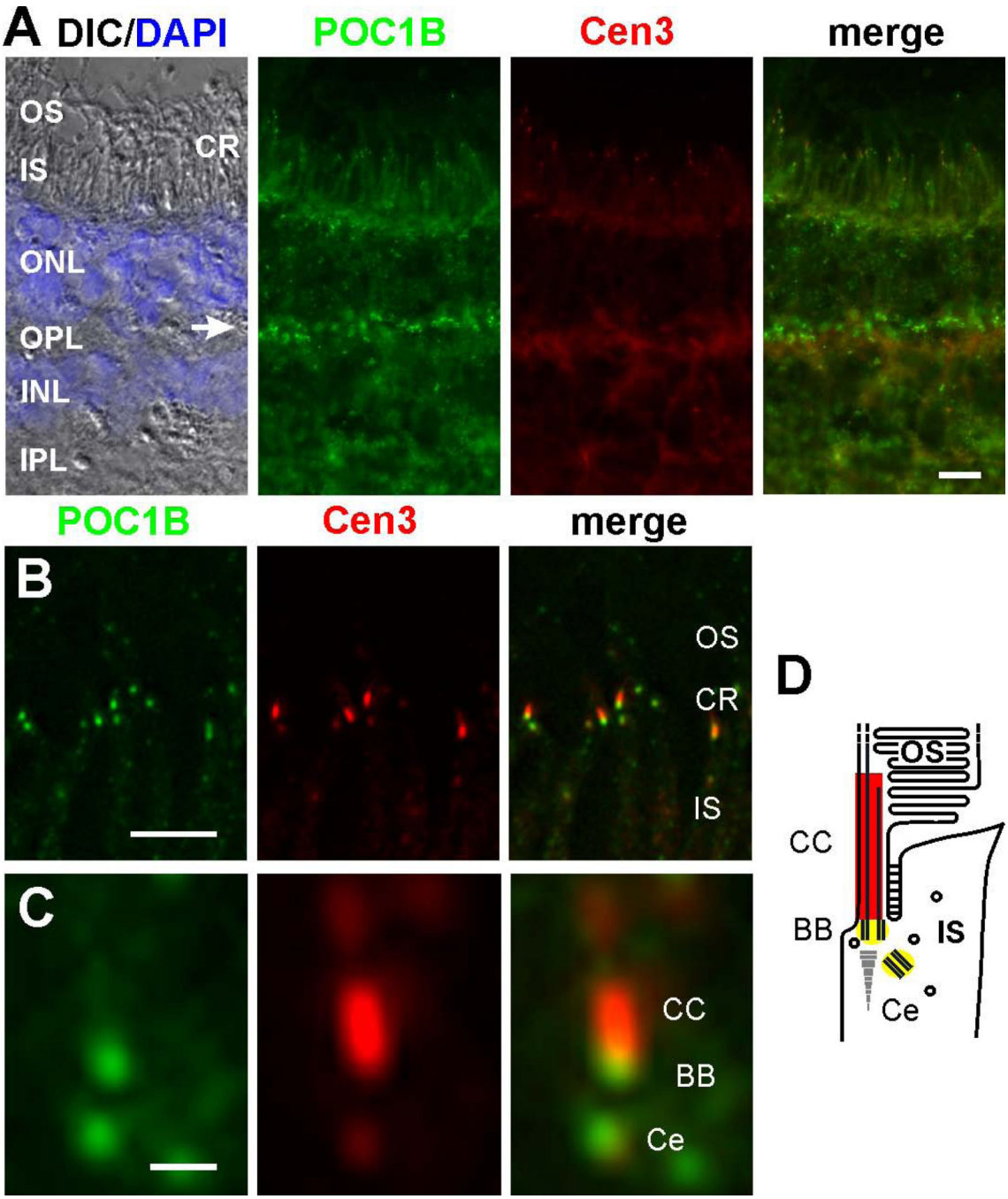

FIGURE 4. Localization of POC1B in the human retina

A Longitudinal cryosections through a human retina stained for POC1B (green) and counterstained for the ciliary marker centrin-3 (Cen3, red) reveals POC1B localization in the ciliary region (CR) of the photoreceptor layer and the synapses of the outer plexiform layer (OPL) (arrow). Overlay of DIC (differential interference contrast) image with DAPI (blue) nuclear stain in the outer (ONL) and inner nuclear layer (INL) shows retina layers. OS, outer segment; IS, inner segment. **B** Increased magnification of the photoreceptor cells demonstrates co-localization of POC1B and Cen3 in the photoreceptor ciliary region (CR).

C High magnification of the photoreceptor cilium reveals substantial localization of POC1B at the centriole (Ce) and the basal body (BB) of the connecting cilium (CC), but not in the CC itself, as schematically demonstrated in **D**. Scale bars: A, 10 μm; B, 5 μm; C, 0.5 μm.

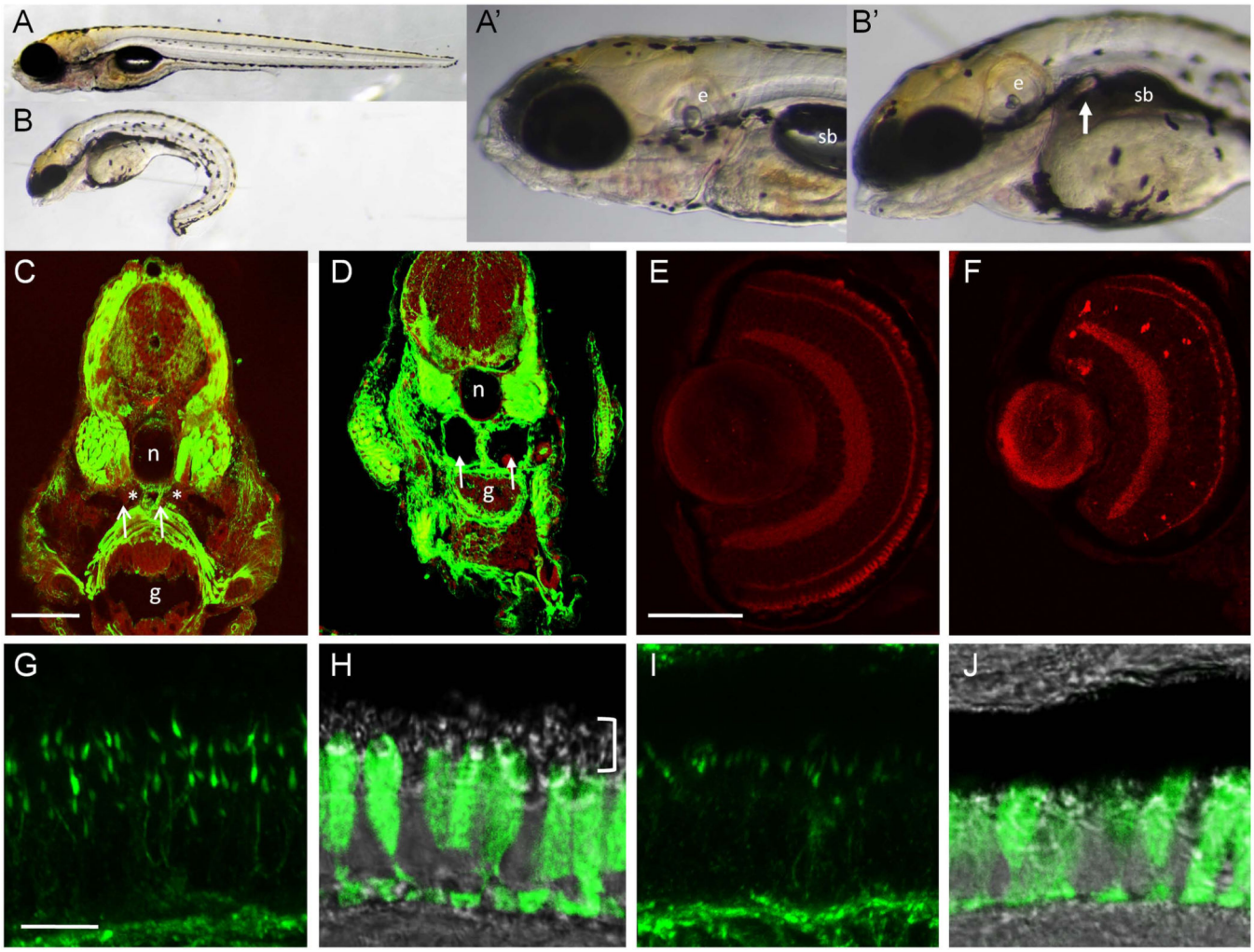

FIGURE 5. Morpholino knockdown of zebrafish *poc1b* results in photoreceptor abnormalities and retinal cell death

A – B whole 5dpf larvae, lateral views. **A'**, **B'** High magnification views of the animals pictured in A and B. Compared to controls (**A**), morpholino treated larvae (**B**) have curved body axes, small eyes and heads and reduced body length. The swim bladder (sb) does not inflate in *poc1b* morphants and kidney cysts are observed in a subset of *poc1b*MO animals (white arrow in B'). **C – D** Transverse sections through the trunk region of 4dpf control (**C**) and morphant (**D**) larvae labeled with actin (green) and TOPRO3 (red). Pronephric ducts are indicated with asterisks in C; white arrowheads indicate kidney cysts in the *poc1b*MO animal. **E – F** Retinal cell death in *poc1b*MO larvae. Sectioned retinal tissue from 5dpf control animals (**E**) labeled with Caspase-3 (red) are negative for retinal cell death at this stage. Some autofluorescence is present in the photoreceptor outer segments. *poc1b*MO retinal sections (**F**) show normal retinal cell layers but smaller eye size relative to controls and an increase in retinal cell death, primarily in the inner nuclear layer. **G – J** Photoreceptor connecting cilia and outer segments are abnormal in *poc1b* morphants. Compressed 10μm z-stack of retinas stained with acetylated tubulin (**G, I**) show the tiered arrangement and length of connecting cilia in control retinas (G). Cilia are reduced in length

and number in the morphant retinas (**I**). Green signal at the base of the images marks the outer plexiform layer. **H, J** The zpr1 antibody (green) labels the inner segments of the long red/green double cones. Uniform distribution of zpr1 from pedicles to the top of the inner segment is observed in controls (**H**). DIC imaging shows cone outer segments (white bracket) superior to the zpr1 label and inferior to the retinal pigmented epithelium. In *poc1b* morphants (**J**), inner segments appear somewhat reduced by zpr1 labeling, and few outer segments are observed by DIC. Scale bars: C–F: 50 μm; G–J: 10 μm. e, ear; sb, swim bladder; n, notochord; g, gut.